Detecting Root Rot Infected Norway Spruce Trees Using Multispectral and LiDAR UAV Data

Gustav Boman ¹, Basam Dahy ², Esra Sengun ², Johanna Witzell ², Johan E. S. Fransson ²

¹ Department of Biology and Environmental Science, Linnaeus University, Kalmar, Sweden – gust.boman@gmail.com
² Department of Forestry and Wood Technology, Linnaeus University, Växjö, Sweden – bassam.saeed@lnu.se, esra.sengun@lnu.se, johanna.witzell@lnu.se, johan.fransson@lnu.se

Keywords: Multispectral Imaging, LiDAR Intensity, Sustainable Forest Management, Precision Forestry, UAV-Based Monitoring.

Abstract

Root rot caused by fungi in the *Heterobasidion* spp. and *Armillaria* spp. is one of the most economically significant problems in the European forest industry. Early detection remains challenging due to the lack of external visual symptoms in infected trees. This study explores the potential of unmanned aerial vehicles (UAVs) equipped with multispectral and light detection and ranging (LiDAR) sensors for detecting spectral and structural differences between healthy and root rot-infected Norway spruce (*Picea abies* (L.) H. Karst.) trees growing in southern Sweden. Remote sensing data from a total of 110 trees, classified as healthy (n=59) or infected (n=51) based on post-harvest survey of stump decay, were analysed. Canopy multispectral reflectance values from red, green, red-edge and near-infrared (NIR) bands, as well as from the reflected intensity values from the point cloud of LiDAR data, were analysed based on pre-harvest remote sensing data. Statistical analysis revealed significant differences in spectral response between healthy and infected trees in both the NIR band from the multispectral data and the reflected intensity from the LiDAR point cloud. These results underscore the potential of UAV-based optical and LiDAR data for detecting forest pathogen damage, highlighting their value in supporting sustainable and effective forest management.

1. Introduction

Root rot has a significant economic impact and is estimated to cost the European forest industry at least 800 million Euro annually (Asiegbu et al., 2005). The damage is primarily caused by fungal pathogens from Heterobasidion spp. and Armillaria spp. (Solheim, 2010). Trees attacked by these fungi via roots exhibit symptoms such as crown thinning and decay in the heartwood and roots (Asiegbu et al., 2005; Dalponte et al., 2022; Kurkela 2002). When faced with pathogenic attacks, trees can divert resources from biomass production towards defence mechanisms. Tree defences against pathogens include both constitutive defences, such as bark and lignin, and inducible defences, like the production of pathogenesis-related proteins and the formation of traumatic resin ducts that are activated following infection (Mageroy et al., 2023). These strategies ensure both immediate and long-term protection. The trade-off between growth and defence may limit the competitive success of the trees (Herms and Mattson, 1992). Moreover, both decay and reduced biomass production can significantly diminish the economic profit from the affected forest stand.

Early detection of infected trees is essential for effective forest management and mitigation strategies, as well as for estimating the financial impact of root rot damage before final harvesting. A major challenge in the early detection of rot infected trees lies in the absence of external visible symptoms (Vollbrecht and Agestam, 1995). Remote sensing techniques have shown promising results in identifying tree stress before visible signs appear, including water stress, nutrient levels, and bark beetle infestations (Behmann et al., 2014; Meddens et al., 2013; Peng et al., 2020). The red-edge band (680-750 nm), for example, can detect chlorophyll concentrations in leaves and pine needles (Gitelson et al., 1996). In the visible range, reflectance is largely influenced by the concentration of chlorophyll and other pigments. Chlorophyll absorbs blue and red wavelengths, resulting in low reflectance in these bands. As pigment absorption is minimal in the NIR, healthy vegetation typically

exhibits high reflectance in this spectral band (Male et al., 2010). Although numerous remote sensing studies have focused on evaluating general vegetation health and stress levels, the application of these techniques for early detection of rot infected trees remains comparatively underexplored. Light detection and ranging (LiDAR) data can be used to estimate structural attributes of individual trees, such as crown width, diameter, volume, and height (Maltamo et al., 2004), but the reflected light from each point in the LiDAR point cloud could potentially also be used for detection of damage. The ability of LiDAR to capture three-dimensional canopy structure, along with spectral values of reflected light, opens new possibilities for detecting structural differences between healthy and infected trees. Thus, data acquisition using sensors mounted on unmanned aerial vehicles (UAVs) provides a potential method for assessing forest health on a large scale and at a low cost. This study explores whether root rot in Norway spruce (Picea abies (L.) H. Karst.) trees can be detected through spectral and structural differences captured by multispectral and LiDAR UAV data.

2. Materials and Methods

2.1 Remote Sensing Data

Multispectral images and LiDAR point cloud data were collected on October 6, 2024, using a DJI Mavic 3M drone equipped with a multispectral (four lenses) camera and an RGB camera (i.e., 4×5 MP in green, red, red-edge, and near-infrared and 20 MP in RGB) (DJI, 2024a), and a DJI Matrice 350 RTK drone equipped with a DJI Zenmuse L2 sensor (i.e., a Livox LiDAR module and a 20 MP RGB camera) (DJI, 2024b), respectively. The UAV campaigns were conducted over a forest stand (~ 2 ha) prior to tree felling and post harvesting. The post-harvest campaign provided an overview of the harvested area and a background image for superimposing GNSS-measurements of tree stump positions (Figure 1). Weather conditions during all drone flights were sunny with some cloud cover. The flights in fall of 2024 were carried out at an altitude of about 60 m above ground level



Figure 1. Post harvest UAV image of the study area at the estate Pukatorp 1:1 (March 2025).

and at a speed of 4 m/s. The multispectral imagery was captured with a frontal overlap of 80% and a side overlap of 70%, while the LiDAR data were collected with a side overlap of 60%, ensuring high spatial resolution and a dense point cloud. The spatial resolution for the multispectral data was 2.77 cm (ortho ground sampling distance) and the density of the LiDAR point cloud reached about 250 points per square meter.

2.2 Field Data

This study was conducted on the estate Pukatorp 1:1, located about 20 km northeast of Växjö (56°59'11.0"N, 15°03'00.1"E) in

southern Sweden. Field data were collected to classify healthy trees from trees with rot. Stumps were surveyed in March 2025, after tree harvesting to determine infection status (Figure 2), stump diameter, and stump position. The latter were measured with a high-precision GNSS receiver (Trimble R12i) in RTK mode to obtain sub-centimetre accuracy. The stump diameter was measured as an auxiliary variable to evaluate potential differences in UAV data between thinner (suppressed trees) and thicker (dominant) trees.



Figure 2. Examples of a healthy (left) and a root rot-infected (right) Norway spruce (*Picea abies* (L.) H. Karst.) stump.

Based on the stump survey, the spectral reflectance responses in the tree crowns could be compared between healthy and infected trees, focusing on the following wavelengths: green (G): 560 ± 16 nm, red (R): 650 ± 16 nm, red-edge (RE): 730 ± 16 nm, and near-infrared (NIR): 860 ± 26 nm. In addition, reflected light from each point in the LiDAR point cloud was acquired at a wavelength of 905 nm.

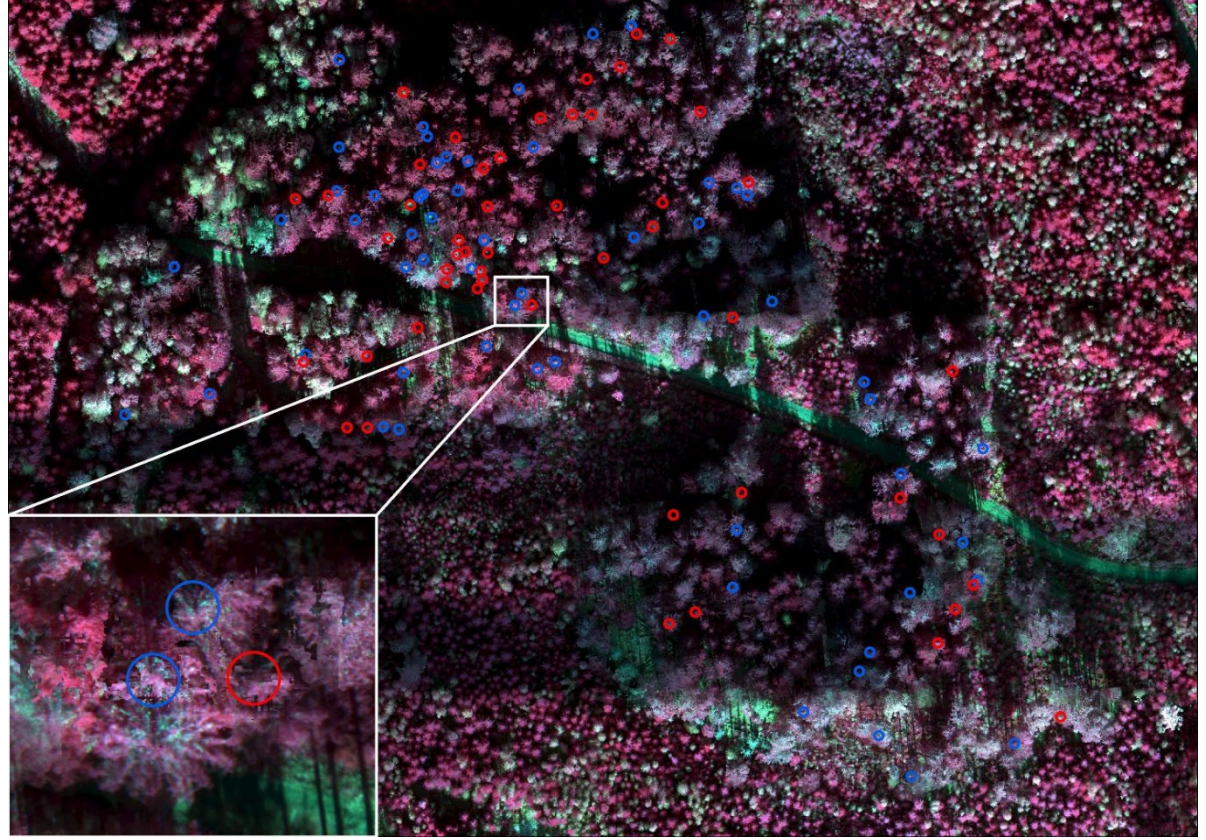


Figure 3. Near-infrared false colour composite image covering the forest stand, where lighter parts represent higher reflectance values and darker parts lower reflectance values. The circles are located around each selected tree crown used in this study. To the bottom left a magnified view of three of the circles are shown, where red circle is located on infected trees and blue circles are located on healthy trees.

2.3 GIS and Statistical Analysis

GIS-based spatial analysis was performed using ArcGIS Pro to compare spectral reflectance responses from the tree crowns across the mentioned wavelengths on the healthy and infected trees, determined from the stump survey, within the forest stand. Two buffer zones with a radius of 0.5 m and 1.0 m were created around each tree crown position using the GNSS-measured stump positions from the field survey post harvesting (see Figures 4 and 5). These buffer zones were then used to extract mean spectral reflectance values for each tree location. The values were extracted for the four spectral bands R, G, RE, and NIR, as well as for the LiDAR point cloud. A total of 59 healthy and 51 infected trees were included in the analysis. As a LiDAR point cloud can be used to delineate tree crowns, it was also used to assist in locating the 110 tree crowns assumed to be in the vicinity of the positions measured from the stump survey post harvesting using the GNSS-receiver, for extracting the spectral reflectance values (Reutebuch et al., 2003). Prior to statistical testing of differences between healthy and infected trees, a Levene's test was conducted to assess the assumption of equal variances for both multispectral and LiDAR data. For the multispectral data, the assumption of equal variances was met and, therefore, a Student's t-test was used to compare the mean spectral values between healthy and infected trees. As for the LiDAR data, the values showed unequal variance between the groups and, thus, a Welch two sample t-test, which does not assume equal variance, was used for those comparisons. Lastly, to further explore potential spectral differences, a closer examination was performed on the forty trees exhibiting the highest and lowest mean spectral values.

3. Results

A statistically significant difference was found in the NIR band between healthy and root rot-infected trees when using a 0.5 m buffer zone around the center points of the treetops (t_{108} =2.3; p=0.0244). The red-edge and green bands showed a declining trend, but no significant difference was found between the infected and healthy trees (t_{108} =1.5; p=0.1514; t_{108} =1.5; p=0.1853, respectively), while the red band had the highest p-value of all spectral bands (t_{108} =0.5; p=0.6378). These patterns are visualised in Figure 6, which shows the mean spectral response distributions as a boxplot for each band. All multispectral p-values were higher when using the 1.0 m buffer and the NIR band was the only one with a significant difference (t_{108} =2.0; p=0.0446).

For the LiDAR data (Figure 7), the 1.0 m buffer resulted in a lower *p*-value (t_{108} =2.2; p=0.0312), compared to the 0.5 m buffer (t_{108} =1.6; p=0.1065). There was no significant difference in stump diameter between healthy and infected trees (t_{108} =0.7; p=0.4509) (Figure 8).

For NIR, out of the twenty trees with the highest mean spectral reflectance values for the 0.5 m buffer, thirteen were classified as healthy and nine out of the twenty trees with the lowest spectral reflectance values were also classified as healthy. When the same comparison was made for LiDAR using the 1.0 m buffer, half of the twenty trees with the highest mean spectral reflectance was healthy and five out of the twenty trees with the lowest mean spectral reflectance was healthy.

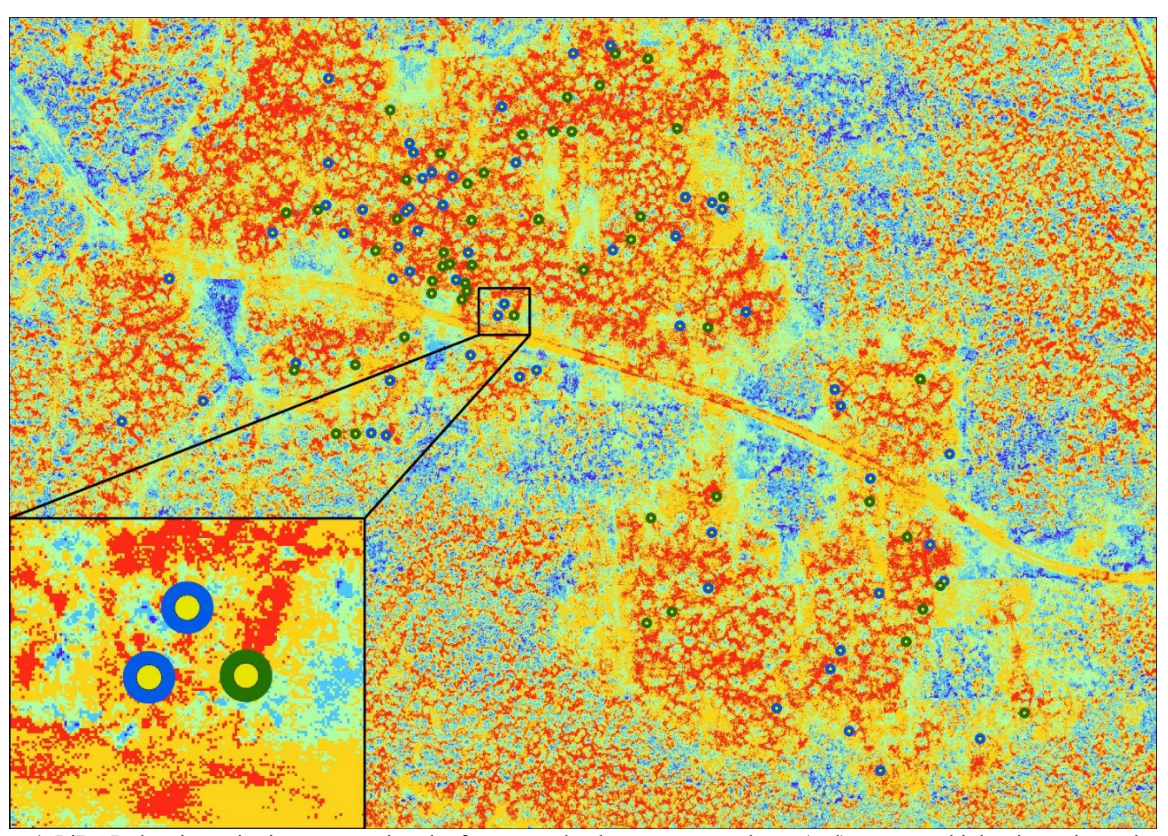


Figure 4. LiDAR data intensity image covering the forest stand, where warmer colours (red) represent higher intensity and cooler colours (blue) indicating lower intensity. The two circles for each dot are the buffer zones retrieved from the GNSS-measured tree stumps representing the tree crowns. To the bottom left a magnified view of three of the buffer zones are shown, where yellow circle is the 0.5 m buffer zone, and green (infected) and blue (healthy) is the 1.0 m buffer zone used for spatial analysis of spectral reflectance.

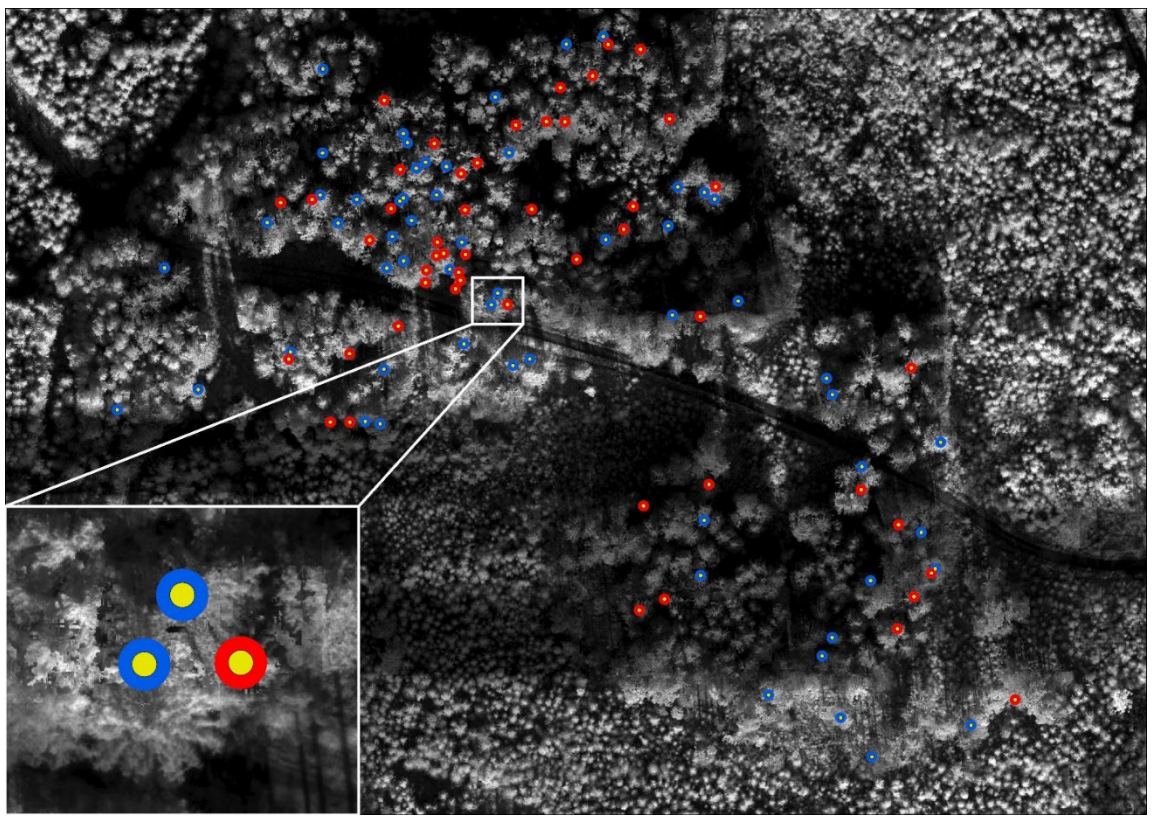


Figure 5. NIR spectral reflectance image covering the forest stand, where lighter parts represent higher reflectance values and darker parts lower reflectance values. The two circles for each dot are the buffer zones retrieved from the GNSS-measured tree stumps representing the tree crowns. To the bottom left a magnified view of three of the buffer zones are shown, where yellow circle is the 0.5 m buffer zone, and red (infected) and blue (healthy) is the 1.0 m buffer zone used for spatial analysis of spectral reflectance.

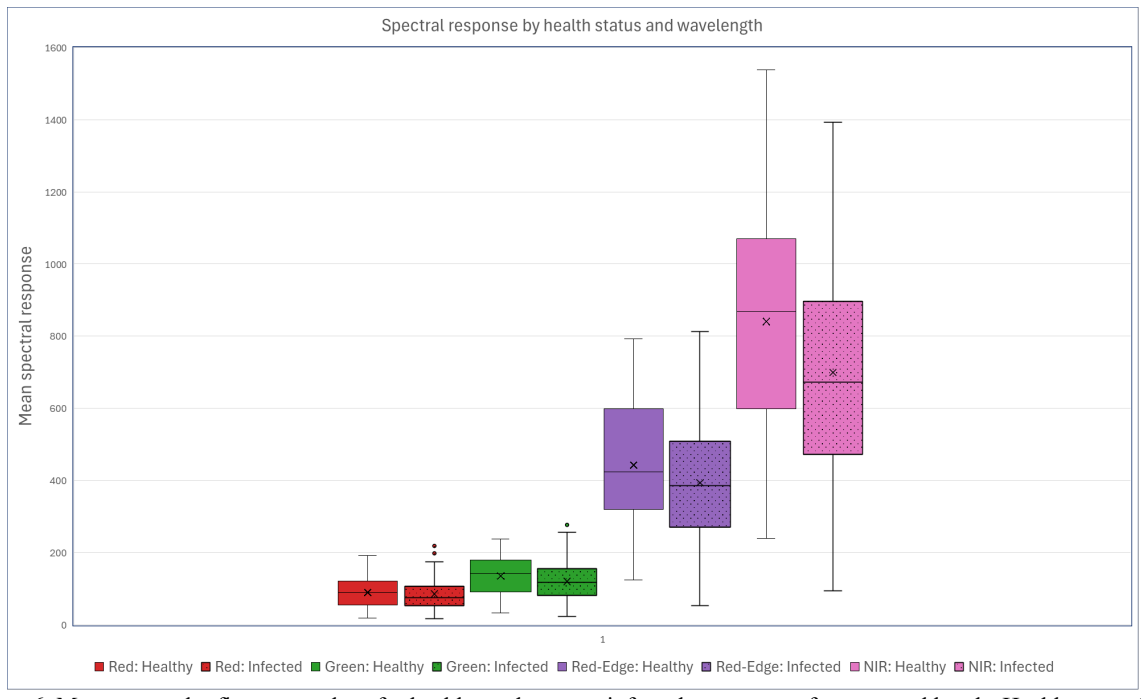


Figure 6. Mean spectral reflectance values for healthy and root rot-infected trees across four spectral bands. Healthy trees (left) consistently show higher reflectance values compared to infected trees (right), particularly in the NIR band. The boxplots show the distribution of mean values within 0.5 m radius buffer zones around each tree crown. Each box represents the interquartile range (25th to 75th percentile), the horizontal line shows the median and the "x" is the mean value of the box plot. The whiskers extend to the minimum and maximum values within 1.5 times the interquartile range. Outliers beyond the whiskers are shown as dots. The statistical analysis for these boxplots was assessed using a Student's t-test.

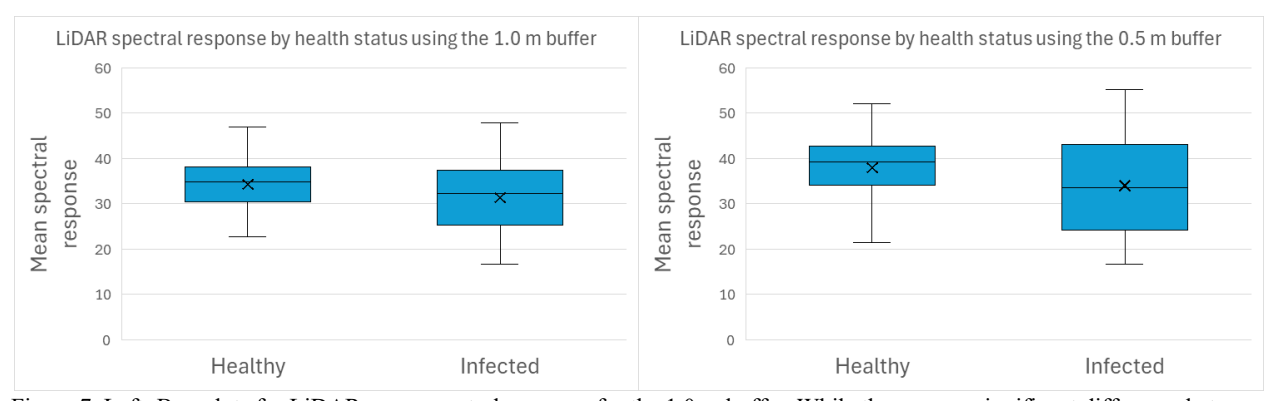


Figure 7. Left: Box plots for LiDAR mean spectral response for the 1.0 m buffer. While there was a significant difference between healthy and root rot-infected trees (t₁₀₈=2.2; p=0.0312), the infected trees (n=51) showed a greater variation of spectral response compared to the healthy trees (n=59). Right: Box plots for LiDAR mean spectral response for the 0.5 m buffer. Unlike the 1.0 m buffer, there was no significant difference in spectral response (t₁₀₈=1.6; p=0.1065), between healthy and infected trees. The statistical analysis for these boxplots was assessed using a Welch t-test.

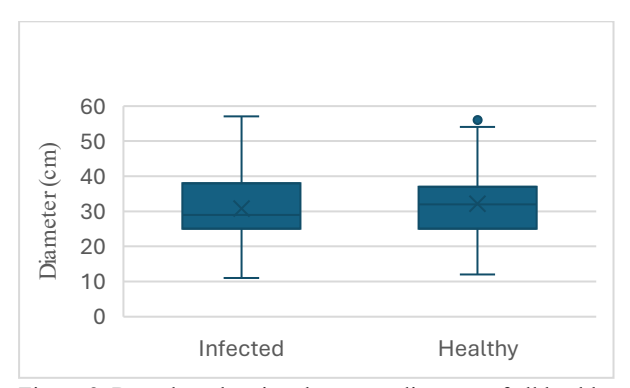


Figure 8. Box plots showing the stump diameter of all healthy and infected trees used in this study. No significant difference $(t_{108}=0.7; p=0.4509)$ was found between the two groups.

4. Discussion

In this study, we addressed the challenge of early detection of fungal infections in Norway spruce trees. Due to the lack of clear external symptoms in early stages, we explored whether spectral and structural differences captured by UAV-based multispectral and LiDAR data could be used to distinguish between healthy and infected trees.

The significant difference observed in the NIR band suggests that this wavelength is effective in discriminating between the spectral reflectance values of healthy trees and those infested with rot. The relatively low *p*-values in red-edge and green bands further suggests that subtle differences in chlorophyll levels in coniferous needles can be detected using these wavelengths (Gitelson et al., 1996). An important spatial consideration in our analysis was the influence of buffer size to extract spectral data from UAV imagery. The lack of significance in the 1.0 m buffer for multispectral data highlights the importance of spatial scale, suggesting that a larger buffer may dilute the spectral response from tree crowns due to mixed pixels from the sunlit and shaded part of the tree crown. Interestingly, the opposite pattern was observed from the spectral response of the LiDAR echo, where the 1.0 m buffer zone yielded a lower p-value compared to the 0.5 m buffer zone. This suggests that structural differences caused by root rot, such as reduced crown density, may be more detectable when using a broader buffer for spatial analysis.

The lower reflectance values observed in NIR and LiDAR data for infected trees may be explained by a reduction of reduced needle mass. As trees with fewer needles have more visible twigs and branches, it is reasonable to assume that the tree crowns have lower spectral reflectance overall. LiDAR, through its sensitivity to three-dimensional canopy structure, may capture early responses to infection not visible in spectral data alone. As this distribution suggests that while there may be a clear relationship between spectral intensity and tree health, the distinction is not always sufficiently clear to serve as a reliable indicator on its own. While previous studies have used LiDAR data to determine tree crown position and structure, none seem to have explored the potential of using the reflected intensity from the LiDAR point cloud data for detecting rot infection (Asiegbu et al., 2005; Dalponte et al., 2022; Kurkela, 2002). This study, therefore, contributes to an unexplored use of LiDAR data in detecting root rot in Norway spruce trees.

5. Conclusions and Future Work

The results of our study demonstrate that UAV-based multispectral imaging, particularly through NIR reflectance at the tree crown level, and LiDAR spectral reflectance from the point cloud can be used to detect signs of root rot in single trees of Norway spruce. The sensitivity of LiDAR to both vertical and horizontal structural variation in terms of canopy density, may offer valuable insights into crown shape characteristics associated with infection that could not be captured using optical data.

Future research should further explore the predictive power of NIR and LiDAR-based metrics, separate and in combination, with the aim of identifying infected trees prior to tree felling. Ultimately, this approach could contribute to the development of effective mapping and monitoring of root rot in Norway spruce using high-resolution remote sensing data within the European forest industry. To ensure the operational utility of this approach in forest health monitoring, future studies should also address the critical need for non-destructive ground-truthing methods. Developing and validating such techniques will be essential for applying this methodology to live, standing forests, thereby expanding its relevance for sustainable forest management. In future work, we will also quantitatively compare the data from the DJI Mavic 3M RGB camera and the RGB data from the DJI Zenmuse L2 sensor to evaluate the additional value.

Acknowledgements

This research was carried out as part of the program Future Forest Management in Southern Sweden (FRAS II) and also received support from The Bridge, a unique partnership between Södra, IKEA, and Linnaeus University that unites academia and industry for innovation and sustainability, focusing on forestry and wood, and the Brattås Foundation for Forest Science Research. The authors gratefully acknowledge the financial support provided by these initiatives, which made this study possible. The contributions have been instrumental in fostering interdisciplinary collaboration and advancing research on sustainable forest management and environmental monitoring.

References

Asiegbu, F. O., Adomas, A., & Stenlid, J. A. N., 2005. Conifer root and butt rot caused by Heterobasidion annosum (Fr.) Bref. sl. *Molecular plant pathology*, *6*(4), 395-409. https://doi.org/10.1111/j.1364-3703.2005.00295.x

Behmann, J., Steinrücken, J., & Plümer, L., 2014. Detection of early plant stress responses in hyperspectral images. *ISPRS Journal of Photogrammetry and Remote Sensing*, *93*, 98-111. https://doi.org/10.1016/j.isprsjprs.2014.03.016

Dalponte, M., Solano-Correa, Y.T., Ørka, H.O., Gobakken, T., Næsset, E., 2022. Detection of heartwood rot in Norway spruce trees with lidar and multi-temporal satellite data. International Journal of Applied Earth Observation and Geoinformation, 109, 102790. https://doi.org/10.1016/j.jag.2022.102790

DJI. (2024a). *DJI Mavic 3M user manual (v1.8)*. https://dl.djicdn.com/downloads/DJI_Mavic_3_Enterprise/2024 0814/DJI_Mavic_3M_User_Manual_EN.pdf

DJI. (2024b). Zenmuse L2 user manual (v1.2). https://dl.djicdn.com/downloads/Zenmuse_L2/20240718/Zenmuse L2 User Manual v1.2 ENI.pdf

Mageroy, M. H., Nagy, N. E., Steffenrem, A., Krokene, P., & Hietala, A. M., 2023. Conifer defences against pathogens and pests—mechanisms, breeding, and management. *Current Forestry Reports*, *9*(6), 429-443. https://doi.org/10.1007/s40725-023-00201-5

Gitelson, A.A., Merzlyak, M.N., Lichtenthaler, H.K., 1996. Detection of red edge position and chlorophyll content by reflectance measurements near 700 nm. Journal of Plant Physiology, 148(3-4), 501-508. https://doi.org/10.1016/S0176-1617(96)80285-9

Herms, D.A., Mattson, W.J., 1992. The dilemma of plants: to grow or defend. The Quarterly Review of Biology, 67(3), 283-335. https://doi.org/10.1086/417659

Peng, Y., Zhang, M., Xu, Z., Yang, T., Su, Y., Zhou, T., ... & Lin, Y., 2020. Estimation of leaf nutrition status in degraded vegetation based on field survey and hyperspectral data. *Scientific Reports, 10*(1), 4361. https://doi.org/10.1038/s41598-020-61294-7

Male, E.J., Pickles, W.L., Silver, E.A., Hoffmann, G.D., Lewicki, J., Apple, M., Repasky, K., Burton, E.A., 2010. Using hyperspectral plant signatures for CO2 leak detection during the 2008 ZERT CO2 sequestration field experiment in Bozeman, Montana. Environmental Earth Sciences, 60, 251-261. https://doi.org/10.1007/s12665-009-0372-2

Maltamo, M., Eerikäinen, K., Pitkänen, J., Hyyppä, J., & Vehmas, M., 2004. Estimation of timber volume and stem density based on scanning laser altimetry and expected tree size distribution functions. *Remote sensing of environment, 90*(3), 319-330. https://doi.org/10.1016/j.rse.2004.01.006

Meddens, A. J., Hicke, J. A., Vierling, L. A., & Hudak, A. T., 2013. Evaluating methods to detect bark beetle-caused tree mortality using single-date and multi-date Landsat imagery. *Remote Sensing of Environment*, 132, 49-58. https://doi.org/10.1016/j.rse.2013.01.002

Reutebuch, S. E., McGaughey, R. J., Andersen, H. E., & Carson, W. W., 2003. Accuracy of a high-resolution lidar terrain model under a conifer forest canopy. *Canadian journal of remote sensing*, 29(5), 527-535. https://doi.org/10.5589/m03-022

Solheim, H., 2010. Råtesopper – I levende trær. https://core.ac.uk/reader/285989270

Vollbrecht, G., Agestam, E., 1995. Identifying butt rotted Norway spruce trees from external signs. https://www.cabidigitallibrary.org/doi/full/10.5555/1996060854